

Enhancement of electron correlation due to the molecular dimerization in organic superconductors β -(BDA-TTP) $_2X$ ($X=I_3, SbF_6$)

Hirohito Aizawa*

Institute of Physics, Kanagawa University, Yokohama, Kanagawa 221-8686, Japan

Kazuhiko Kuroki

Department of Physics, Osaka University, Toyonaka, Osaka 560-8531, Japan

Jun-ichi Yamada

Department of Material Science, University of Hyogo, Ako-gun, Hyogo 678-1297, Japan

(Dated: May 26, 2021)

We perform a first principles band calculation for quasi-two-dimensional organic superconductors β -(BDA-TTP) $_2I_3$ and β -(BDA-TTP) $_2SbF_6$. The first principles band structures between the I_3 and SbF_6 salts are apparently different. We construct a tight-binding model for each material which accurately reproduces the first principles band structure. The obtained transfer energies give the differences such as (i) larger dimerization in the I_3 salt than the SbF_6 salt, and (ii) different signs and directions of the inter-stacking transfer energies. To decompose the origin of the difference into the dimerization and the inter-stacking transfer energies, we adopt a simplified model by eliminating the dimerization effect and extract the difference caused by the inter-stacking transfer energies. From the analysis using the simplified model, we find that the difference of the band structure comes mainly from the strength of dimerization. To compare the strength of the electron correlation having roots in the band structure, we calculate the physical properties originated from the effect of the electron correlation such as the spin susceptibility applying two particle self-consistent (TPSC) method. We find that the maximum value of the spin susceptibility of the I_3 salt is larger than that of the SbF_6 salt. Hypothetically decreasing the dimerization within the model of the I_3 salt, the spin susceptibility takes almost the same value as that of the SbF_6 salt for the same magnitude of the dimerization. We expect that the different ground state between the I_3 and SbF_6 salt mainly comes from the strength of the dimerization which is apparently masked in the band calculation along a particular k -path.

I. INTRODUCTION

There have been attempts to synthesize strongly correlated electron systems in organic conductors by applying chemical modification to stable metallic donor molecules. For example, there are (*S,S*)-DMBEDT-TTF¹ and *meso*-DMBEDT-TTF², where two methyl groups are attached to BEDT-TTF, and they are pressure-induced superconductors. In the present article, we theoretically study superconductors based on BDA-TTP molecule, which is extended to six-membered-ring from five-membered-ring in the σ -bond framework of BDH-TTP molecule³. The actual materials are β -(BDA-TTP) $_2I_3$ and β -(BDA-TTP) $_2SbF_6$, which will be abbreviated as I_3 and SbF_6 salts, respectively. In both materials, conductive layer is the BDA-TTP layer, and the anion layer separates the adjacent conductive layers as shown in Fig. 1 (a). Molecular configuration in the conductive layer is the β -type as shown in Fig. 1 (b). Both materials consist of the stacking structure of the BDA-TTP molecules. However, they are somewhat different in that the inter-stacking direction is slightly tilted in the I_3 salt, but almost side-by-side for the SbF_6 salt, which will be shown later.

The I_3 salt is an insulator at ambient pressure, and the superconductivity appears around 10 K under hydrostatic pressure of above 10 kbar⁴. Recently, applying

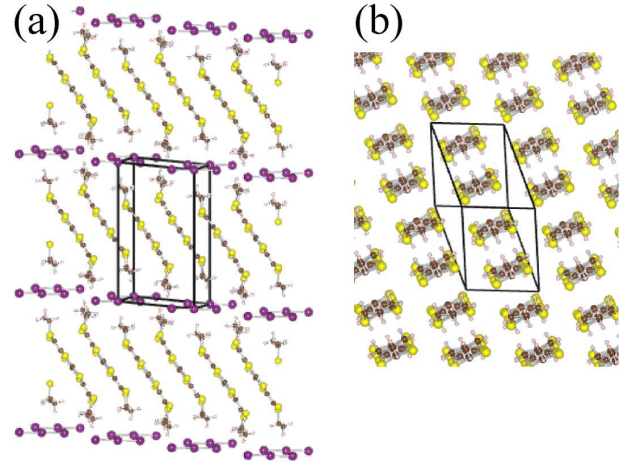


FIG. 1: (color online) Crystal structure of the I_3 salt from (a) the side view and (b) the conductive layer of the BDA-TTP molecules.

uniaxial strain along the c -axis has given higher T_c ⁵. Applying the uniaxial compression once increases the T_c and takes a maximum before it decreases⁶. It is considered that applying the pressure in the I_3 salt increases the overlap between the upper and lower bands, which gradually changes the character of the system from a strongly correlated half-filled system to a moderately correlated

quarter filled system. The c -axis strain more efficiently increases the band-width of the overlap. As the electron correlation is reduced to some extent by pressure, the insulating nature of the material is lost, and superconductivity appears⁵. Theoretically, Nonoyama *et al.* have studied the nature of the charge ordering state and the pairing mechanisms in the model of the I_3 salt derived from the extended Hückel band structure⁷.

The SbF_6 salt exhibits superconductivity at 7.5 K at ambient pressure⁸. As for the SbF_6 salt, there have been some controversies regarding both the anisotropy of the Fermi surface^{9,10} and the directions of the nodes in the superconducting gap^{11–14}. In our previous study¹⁵ for the β -(BDA-TTP)₂ MF_6 ($M=P, As, Sb$ and Ta), we have obtained the band structure from the first principles band calculation, and suggested the origin of the differences from the extended Hückel band structure¹⁶. Also, there have been some studies on pairing mechanisms mediated by spin and/or charge fluctuations in the model of β -(BDA-TTP)₂ X . As for the MF_6 ($M=As, Sb$) salts, adopting models derived from the extended Hückel calculation, Nonoyama *et al.*²⁰ have applied random phase approximation (RPA) to the two band model, while Suzuki *et al.*²¹ have applied the fluctuation exchange (FLEX) approximation to the original two-band model and the single-band dimer model. Recently, we have constructed the tight-binding model derived from the first principles band calculation, studied the pairing symmetry of the gap function within the spin fluctuation mediated pairing¹⁵.

In the present study, given the difference in the ground state between the I_3 salt and the SbF_6 salt, we focus on the difference in the electronic structure between the two salts. In fact, despite the similar lattice structure, the band structure of the I_3 salt⁴ and that of the SbF_6 salt⁸ obtained by the extended Hückel method are known to be very different. Here, we perform the first principles band calculation for β -(BDA-TTP)₂ I_3 and construct an effective tight-binding model that reproduces the first principles band structure. We compare the band structure of the I_3 salt to that of the SbF_6 salt obtained in our previous study¹⁵, and pin down the origin of the apparently large differences. In particular, we study the relation between the strength of the electron correlation and the molecular dimerization. We consider the Hubbard model by introducing repulsive interaction between the electrons on the same BDA-TTP molecule. Then, we study the effect of the electron correlation by applying the two particle self-consistent (TPSC) method, and present quantities such as the spin susceptibility against the temperature and dimerization strength, which reflect physical properties originating from the electron correlation. We conclude that the ground state of the I_3 salt differs from that of the SbF_6 salt due to the strength of the dimerization.

II. METHOD

A. first principles band calculation and model construction

We perform first principles band calculation using all-electron full potential linearized augmented plane-wave (LAPW) + local orbitals (lo) method within the framework of WIEN2k²². This implements the density functional theory (DFT) with different possible approximation for the exchange correlation potentials. The exchange correlation potential is calculated using the generalized gradient approximation (GGA).

The single-particle wave functions in the interstitial region are expanded by plane waves with a cut-off of $R_{MT}K_{max} = 3.0$ due to the presence of the hydrogen atom, where R_{MT} denotes the smallest muffin-tin radius and K_{max} is the maximum value of K vector in the plane wave expansion. In the I_3 salt, the muffin-tin radii are assumed to be 2.50, 1.62, 1.15, and 0.62 atomic units (a.u.) for I, S, C, and H, respectively. K_{max} is taken as 4.8, and the plane wave cutoff energy is 318.6 eV. In the SbF_6 salt, the muffin-tin radii are assumed to be 1.74, 1.74, 1.62, 0.83, and 0.45 a.u. for Sb, F, S, C, and H, respectively. K_{max} is taken as 6.7, and the plane wave cutoff energy is 604.7 eV. Calculations were performed using $6 \times 3 \times 9$ k -points for the I_3 salt and $7 \times 3 \times 9$ k -points for the SbF_6 salt in the irreducible Brillouin zone. We adopt the lattice structure determined experimentally for each materials^{4,8}, and we do not relax the atomic positions in the calculation.

Having done the first principles band calculation, we then construct a tight-binding model which accurately reproduces the first principles band structure. From the lattice structure of the two materials, we regard one molecule as a site and consider a two-band (two sites per unit cell) tight-binding model to fit the first principles band structure. The tight-binding Hamiltonian, H_0 , is written in the form

$$H_0 = \sum_{\langle i\alpha:j\beta \rangle, \sigma} \left\{ t_{i\alpha:j\beta} c_{i\alpha\sigma}^\dagger c_{j\beta\sigma} + \text{H.c.} \right\}, \quad (1)$$

where i and j are unit cell indices, α and β specifies the sites in a unit cell, $c_{i\alpha\sigma}^\dagger$ ($c_{i\alpha\sigma}$) is a creation (annihilation) operator with spin σ at site α in the i -th unit cell, $t_{i\alpha:j\beta}$ is the electron transfer energy between (i, α) site and (j, β) site, and $\langle i\alpha:j\beta \rangle$ represents the summation over the bonds corresponding to the transfer.

By Fourier transformation, eq. (1) is rewritten as

$$H_0 = \sum_{\mathbf{k}, \sigma, \alpha, \beta} \varepsilon_{\alpha\beta}(\mathbf{k}) c_{\mathbf{k}\alpha\sigma}^\dagger c_{\mathbf{k}\beta\sigma}, \quad (2)$$

where $\varepsilon_{\alpha\beta}(\mathbf{k})$ is the site-indexed kinetic energy represented in \mathbf{k} -space. The band dispersion is given by diagonalizing the matrix $\varepsilon_{\alpha\beta}(\mathbf{k})$,

$$\varepsilon_{\alpha\beta}(\mathbf{k}) = \sum_{\gamma} d_{\alpha\gamma}(\mathbf{k}) d_{\beta\gamma}^*(\mathbf{k}) \xi_{\gamma}(\mathbf{k}), \quad (3)$$

where $\xi_\gamma(\mathbf{k})$ gives the band dispersion of the γ -th band measured from the chemical potential, and $d_{\alpha\gamma}(\mathbf{k})$ is the unitary matrix that gives the unitary transformation.

We adopt the two-band Hubbard model obtained by adding the on-site (intra-molecule) repulsive interaction to the tight-binding model derived from the fitting of the first principles band structure. The Hubbard Hamiltonian, H , is

$$H = H_0 + \sum_{i\alpha} U_0 n_{i\alpha\uparrow} n_{i\alpha\downarrow} \quad (4)$$

where U_0 is the bare on-site interaction and $n_{i\alpha\sigma}$ is the number operator of the electron on the α -site in the i -th unit cell. Since both salts are configured as a form of D_2X where D is the donor molecule and X^{-1} is the anion, the band-filling is 1/4-filled in the hole representation (3/4-filled in the electron representation).

B. Two particle self consistent method

To deal with the electron correlation effect arising from the on-site repulsion, we apply TPSC to the multi-site Hubbard model given by eq. (4) as follows. The bare susceptibility in the site-representation is given by

$$\chi_{\alpha\beta}^0(q) = -\frac{T}{N_c} \sum_k G_{\alpha\beta}^0(k+q) G_{\beta\alpha}^0(k), \quad (5)$$

where T and N_c are the temperature and the total number of unit cells, respectively, and $G_{\alpha\beta}^0(k)$ is the bare Green's function given as

$$G_{\alpha\beta}^0(k) = \sum_\gamma d_{\alpha\gamma}(\mathbf{k}) d_{\beta\gamma}^*(\mathbf{k}) \frac{1}{i\varepsilon_n - \xi_\gamma(\mathbf{k})}. \quad (6)$$

Here, we introduce the abbreviations $k = (\mathbf{k}, i\varepsilon_n)$ and $q = (\mathbf{q}, i\omega_m)$ for the fermionic and bosonic Matsubara frequencies. The indices $\alpha\beta$ means $(\alpha \beta)$ -element of the matrix such as $\hat{\chi}^0(q)$.

TPSC has been applied to single-site systems^{23,24}, multi-site system,²⁵ and multi-orbital system²⁶. By applying TPSC, we can consider the local vertex correction in both spin and charge channels within a self-consistent procedure. In the TPSC, using the bare susceptibility given by eq. (5), the spin and charge susceptibilities are obtained as

$$\hat{\chi}^{\text{sp}}(q) = \left[\hat{I} - \hat{\chi}^0(q) \hat{U}^{\text{sp}} \right]^{-1} \hat{\chi}^0(q), \quad (7)$$

$$\hat{\chi}^{\text{ch}}(q) = \left[\hat{I} + \hat{\chi}^0(q) \hat{U}^{\text{ch}} \right]^{-1} \hat{\chi}^0(q), \quad (8)$$

where \hat{U}^{sp} (\hat{U}^{ch}) is the local spin (charge) vertex and \hat{I} is the unit matrix. The local vertices are determined by satisfying two sum rules for the local moment such as

$$\frac{2T}{N_c} \sum_q \chi_{\alpha\alpha}^{\text{sp}}(q) = n_\alpha - 2 \langle n_{\alpha\uparrow} n_{\alpha\downarrow} \rangle, \quad (9)$$

$$\frac{2T}{N_c} \sum_q \chi_{\alpha\alpha}^{\text{ch}}(q) = n_\alpha + 2 \langle n_{\alpha\uparrow} n_{\alpha\downarrow} \rangle - n_\alpha^2, \quad (10)$$

where n_α is the particle number at the site α . We have used the relations $n_{\alpha\uparrow} = n_{\alpha\downarrow} = n/2$ and $n_{\alpha\sigma} = n_{\alpha\sigma}^2$ from the Pauli principles.

The local spin vertex \hat{U}^{sp} is related with the double occupancy $\langle n_{\alpha\uparrow} n_{\alpha\downarrow} \rangle$ by the following ansatz

$$U_{\alpha\alpha}^{\text{sp}} = \frac{\langle n_{\alpha\uparrow} n_{\alpha\downarrow} \rangle}{\langle n_{\alpha\uparrow} \rangle \langle n_{\alpha\downarrow} \rangle} U_{\alpha\alpha}^0, \quad (11)$$

where $U_{\alpha\alpha}^0$ is the $(\alpha \alpha)$ -element of the on-site interaction matrix \hat{U}^0 . Equation (11) breaks the particle-hole symmetry and should be used for $n_\alpha \leq 1$. When $n_\alpha > 1$, that can be applied through the particle-hole transformation, then the double occupancy $D_\alpha = \langle n_{\alpha\uparrow} n_{\alpha\downarrow} \rangle$ is given by

$$D_\alpha = \frac{U_{\alpha\alpha}^{\text{sp}}}{U_{\alpha\alpha}^0} \frac{n_\alpha^2}{4} + \left(1 - \frac{U_{\alpha\alpha}^{\text{sp}}}{U_{\alpha\alpha}^0} \right) (n_\alpha - 1) \theta(n_\alpha - 1), \quad (12)$$

where $\theta(x)$ is Heaviside step function. Equations (7)-(11) give a set of the self-consistent equations for the TPSC method. Obtaining the \hat{U}_{sp} and \hat{U}_{ch} , the interaction for the self-energy is obtained as

$$\hat{V}^\Sigma(q) = \frac{1}{2} \left[\hat{U}^{\text{sp}} \hat{\chi}^{\text{sp}}(q) \hat{U}^0 + \hat{U}^{\text{ch}} \hat{\chi}^{\text{ch}}(q) \hat{U}^0 \right]. \quad (13)$$

Using the eq. (13), the self-energy is given by

$$\Sigma_{\alpha\beta}(k) = \frac{T}{N_c} \sum_q V_{\alpha\beta}^\Sigma(q) G_{\alpha\beta}(k-q), \quad (14)$$

and the dressed Green's function is obtained as

$$\hat{G}(k) = \hat{G}^0(k) + \hat{G}^0(k) \hat{\Sigma}(k) \hat{G}(k). \quad (15)$$

Since we need two sites per unit cell, \hat{U}^0 , \hat{U}^{sp} , \hat{U}^{ch} , $\hat{\chi}^0(q)$, $\hat{\chi}^{\text{sp}}(q)$, $\hat{\chi}^{\text{ch}}(q)$, $\hat{V}^\Sigma(q)$, $\hat{\Sigma}(k)$, $\hat{G}^0(k)$ and $\hat{G}(k)$ all become 2×2 matrices. In the present study, the spin susceptibility is obtained as the larger eigenvalue of the 2×2 spin susceptibility matrix. We consider not only the spin susceptibility, but also other physical values such as the local spin vertex and the double occupancy. In the present calculation, we take the system size as 64×64 k -meshes and 16384 Matsubara frequencies.

III. RESULTS

A. first principles band calculation

Figures 2 (a) and (c) show the first principles band structures for the I_3 and the SbF_6 salts. For both materials, the experimental lattice structure at an ambient pressure and room temperature are used. In both of the materials, it can be seen that the highest-occupied molecular orbital (HOMO) is isolated from the lowest-unoccupied molecular orbital (LUMO). Considering this and also the number of donor molecules in a unit cell, we adopt the HOMO and HOMO-1 bands as the target bands to construct an effective tight-binding model.

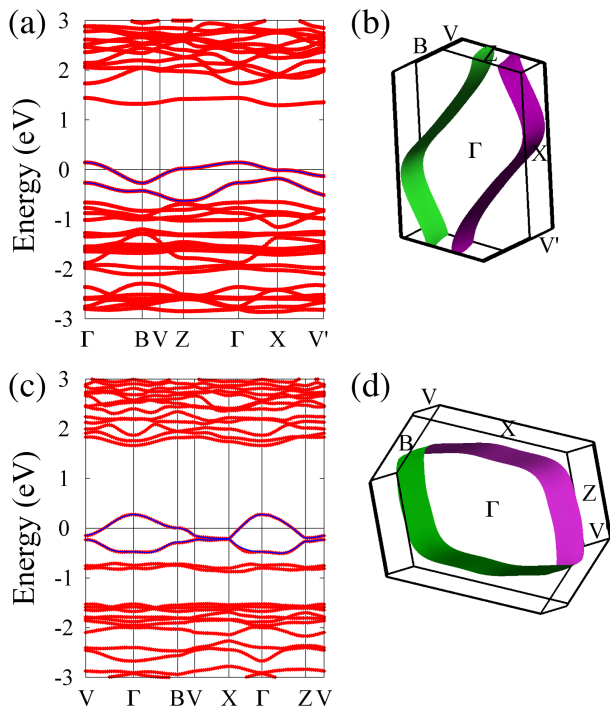


FIG. 2: (color online) (a) Calculated first principles band structure and (b) Fermi surface for the I_3 salt, (c) first principles band and (d) Fermi surface for the SbF_6 salt. In both figures of the band structures, the red curves represent the first principles bands and the blue solid curves gives the tight-binding fit.

Although the difference is only the anion, the band structures of the two materials are apparently very different. In order to reveal the origin of this difference in the band structure, in the following we focus on the following two differences of the two salts. One is the magnitude of the molecular dimerization, namely the dimerization of the donor molecule in the I_3 salt is larger than that in the SbF_6 salt resulting in a larger gap between HOMO and HOMO-1 in the former. The other is the anisotropy of the band structure, namely, there are two flat portions near the Fermi level around the Z and the X-points in the I_3 salt, while there is only one flat portion around the B-point in the SbF_6 salt.

Figure 2 (b) shows the Fermi surface of the first principles band calculation for the I_3 salt, where the high symmetry points in the Brillouin zone are presented only on the $k_Y(k_b) = 0$ plane. The Fermi surface of the I_3 salt is disconnected, namely quasi-one-dimensional, but it is actually close to two dimensional because a slight shift of the band structure around the Z-point would give a closed (i.e. 2D) Fermi surface. Figure 2 (d) shows the Fermi surface of the SbF_6 salt. The Fermi surface is cylindrical, reflecting the two-dimensionality of this salt as shown in our previous work¹⁵.

B. Effective tight-binding model

Figure 3 shows the effective tight-binding model adopted to fit the first principles band. The nearest-neighbor transfers are shown in the left panel of Fig. 3, and in addition we also need to introduce the next-nearest-neighbor transfers shown in the right panel of Fig. 3 to reproduce the first principles band structure more accurately. Note that the stacking direction of the BDA-TTP molecules is taken in the a -direction²⁷. The band dispersions of the tight-binding model are shown as blue solid curves in Fig. 2 (a) for the I_3 salt and Fig. 2 (c) for the SbF_6 salt.

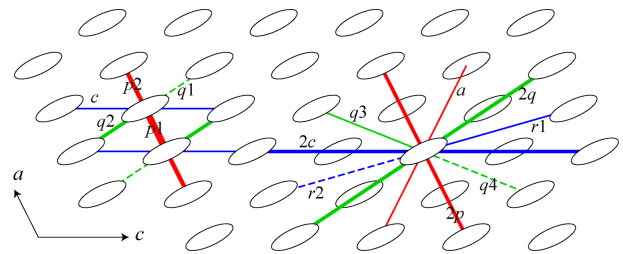


FIG. 3: (color online) The tight-binding model for β -(BDA-TTP) $_2X$, where left (right) panel shows the first (second) nearest-neighbor transfer energies.

The transfer energies for the two salts are summarized in Table I. The bottom three lines represent the magnitude of the dimerization which is measured by the ratio t_{p2}/t_{p1} , and the transfer between the inter-stacking direction normalized by the average value of intra-stacking transfer energies, $(t_{q1} + t_{q2})/(t_{p1} + t_{p2})$ and $2t_c/(t_{p1} + t_{p2})$. From Table I, it can be seen that there are two major differences between the two salts. One is the strength of the molecular dimerization, namely the dimerization in the I_3 salt is larger than that in the SbF_6 salt. Another difference is the transfers in the inter-stacking direction namely, the magnitudes as well as the sign of the inter-stacking transfers are different between the two salts, that is in $c(q)$ -direction in the I_3 (SbF_6) salt.

To clarify the origin of the differences between the two salts, we consider the alignments of the donor molecules in the conducting c - a plane for the two salts. The conducting c - a plane for each salt is shown in Fig. 4. We find that the tilting angle of the donor molecules from the c -axis is different between the two salts. In the I_3 salts shown in Fig. 4 (a), the tilting angle is larger than that in the SbF_6 salts shown in Fig. 4 (b). The difference in the tilting angle gives rise to differences in both the magnitude and the sign of the main inter-stacking transfers, which is t_c in the I_3 salt shown in the lower panel of Fig. 4 (a), while they are t_{q1} and t_{q2} in the SbF_6 salt shown in the lower panel of Fig. 4 (b).

Now, let us try to decompose these differences. We consider a case where we hypothetically eliminate the dimerization effect. Namely, we simplify the model by considering only the nearest neighbor transfer energies,

TABLE I: List of the transfer energies in the unit of eV for β -(BDA-TTP)₂X.

X	I ₃	SbF ₆
t_{p1} (eV)	-0.174	-0.153
t_{p2}	-0.102	-0.126
t_{q1}	0.018	-0.071
t_{q2}	0.041	-0.055
t_c	0.062	0.007
t_{2c}	0.002	0.005
t_{2p}	0.006	0.021
t_a	-0.001	0.003
t_{2q}	0.004	0.005
t_{q3}	-0.012	0.003
t_{q4}	0.013	0.006
t_{r1}	0.002	0.014
t_{r2}	0.009	0.008
t_{p2}/t_{p1}	0.586	0.824
$\frac{t_{q1}+t_{q2}}{t_{p1}+t_{p2}}$	-0.214	0.452
$\frac{2t_c}{t_{p1}+t_{p2}}$	-0.449	-0.050

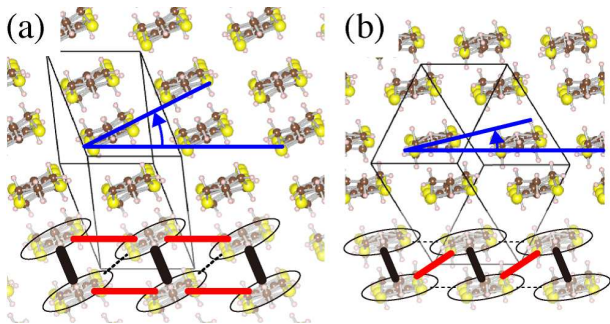


FIG. 4: (color online) The lattice structures of (a) the I₃ and (b) the SbF₆ salt. Blue solid lines represent the tilting angles of the donor molecules, which is measured from the c -direction taken in the horizontal direction. In the lower panel, the ellipses represent the donor molecules, the black solid lines show the intra-stacking transfer, and the red solid (black dotted) lines represent the main (not main) inter-stacking transfer.

and replace the hopping in the p - and q -directions by taking their averages. The band structure of the simplified model is given by

$$\varepsilon(\mathbf{k}) = 2t_c \cos(k_c) + 2t_p \cos(k_a) + 2t_q \cos(k_c + k_d) \quad (6)$$

where the transfer energies are $t_p = -0.138$ eV, $t_q = 0.030$ eV, $t_c = 0.062$ eV for the I₃ salt, and $t_p = -0.140$ eV, $t_q = -0.063$ eV, $t_c = 0.007$ eV for the SbF₆ salt. Eliminating the dimerization effect enables us to take the unit cell reduced along the a -direction. By comparing the band structure of the simplified model, we can extract the difference caused by the inter-stacking transfer.

We compare the band structure of the two salts in the (k_X, k_Y) plane, where k_Y is taken in the molecular stacking direction and k_X is taken in the direction of the main

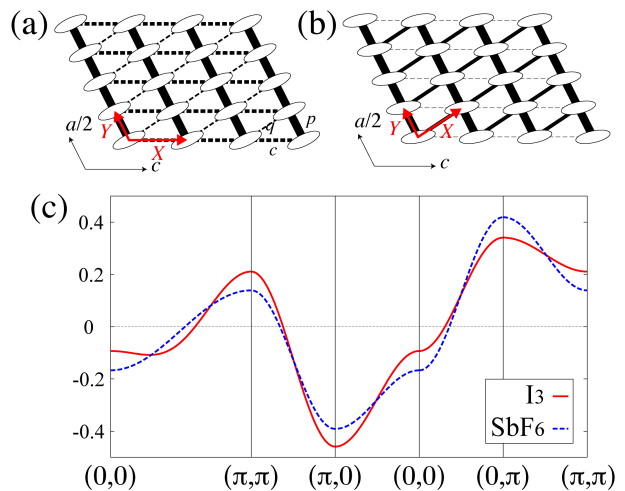


FIG. 5: (color online) The simplified model for (a) the I₃ salt and (b) the SbF₆ salt, where the line width schematically represents the magnitude of the transfer energies, and the solid (dashed) line represents the negative (positive) value of the transfer energies. (c) The band structure of the simplified model by eliminating the dimerization for each salts.

inter-stacking transfer, namely, c -direction in the I₃ salt (Fig. 5 (a)) and $a/2 + c$ -direction in the SbF₆ salt as seen in Fig. 5 (b). Also, we shift the wave-number by $(\pi, 0)$ for the SbF₆ salt considering the sign difference in the main transfer energies along the inter-stacking direction. By such a transformation, we find that the band structures between the I₃ salt and the modified SbF₆ salt become very similar as shown in Fig. 5 (c). Since the simplified model eliminates the dimerization effect, the difference in the original band structure between the two salts *comes mainly from the dimerization*, and the differences coming from the inter-stacking transfer are not essential.

C. Effect of electron correlation cooperating with dimerization

A quarter-filled system effectively becomes a half-filled system by increasing the dimerization²⁸, so that the electron correlation is strengthened. Since we now know that the strength of the dimerization is the essential difference between the I₃ and SbF₆ salts, we expect that the difference of the ground state physical properties between the two salts is caused by the strength of the electron correlation originating from the difference in the strength of the dimerization.

The strength of the electron correlation can be measured by calculating the spin susceptibility. We apply the TPSC scheme to the Hubbard model of the I₃ salt. From the first principles calculation of the I₃ salt, the band width W is about 0.77eV, so we take the on-site interaction $U_0 = 0.8\text{eV}$ as same as the band width. The bare on-site interaction U_0 is estimated in the other strongly correlated organic conductors applying the first-principles

calculation^{29,30}. Referring to them, the on-site interaction we taken is appropriate.

Figure 6 (a) shows the temperature dependence of the local vertex of the spin part U_{sp} and the critical on-site interaction of the magnetic order U_{SDW} in the left scale. Above the temperature $T \approx 0.004\text{eV}$, U_{sp} is almost unchanged and U_{SDW} gradually decreases with lowering the temperature. Below $T \approx 0.004\text{eV}$, U_{sp} takes almost the same value, but somewhat smaller value than U_{SDW} , which can be understood that the magnetic ordering is developed with lowering the temperature.

In the right scale of Fig.6(a), we present the ratio $U_{\text{SDW}}/U_{\text{sp}}$ as a function of T . The TPSC approach satisfies the Mermin-Wagner theorem so the true magnetic ordering does not occur in the present model, but we can regard the temperature at which the line extrapolating $U_{\text{SDW}}/U_{\text{sp}}$ from high temperature reaches unity as the magnetic critical temperature in the actual three dimensional system. We estimate the magnetic critical temperature to be about 0.0038 eV . Reflecting the tendency toward the magnetic ordering, U_{ch} quickly increases below $T = 0.0038\text{ eV}$ as shown in Fig. 6 (b). We show the double occupancy $\langle D \rangle = \langle n_{\uparrow}n_{\downarrow} \rangle$ as a function of T in Fig. 6 (c). Similarly to the local vertices, the double occupancy $\langle D \rangle$ also changes below $T = 0.0038\text{eV}$. Decreasing the temperature reduces the double occupancy, which means the tendency of the magnetic localization at each site. Figure 6 (d) shows the inverse of the maximum value of the spin susceptibility against T . As expected from Fig. 6 (a), the inverse of the spin susceptibility extrapolates to zero around $T = 0.0038\text{ eV}$. In fact, a very recent experiment observes a magnetic transition in the Mott insulating state of the I_3 salt at low temperature³¹. TPSC is not capable of directly describing the magnetic ordering of a Mott insulator, but the very fact that the material is a Mott insulator is consistent with our view that the electron correlation effect is strong due to the strong dimerization.

Figures 7 (a) and (b) show the absolute value of the Green's function $|G|$ and the spin susceptibility χ_{sp} of the I_3 salt with $U_0 = 0.8\text{eV}$ and $T = 0.004\text{eV}$. The absolute value of the Green's function takes large values near the Fermi surface shown in Fig. 7 (a). The wave number at which the spin susceptibility is maximized corresponds to the nesting vector of the Fermi surface as seen in Fig. 7 (b). As shown in Fig. 7 (b), the maximum value of the spin susceptibility takes a large value since its temperature is close to the critical temperature.

To clarify the relation between the electron correlation and the dimerization, we measure the strength of the dimerization by the quantity t_{p2}/t_{p1} . When t_{p2}/t_{p1} goes to unity, the dimerization decreases. If the decrease of the dimerization results in weakening the electron correlation, we expect (i) U_{sp} gradually deviates from U_{SDW} , (ii) the double occupancy $\langle D \rangle$ becomes large, and (iii) the maximum value of the spin susceptibility decreases within the TPSC scheme. Furthermore, if the stronger electron correlation of the I_3 salt originates from the

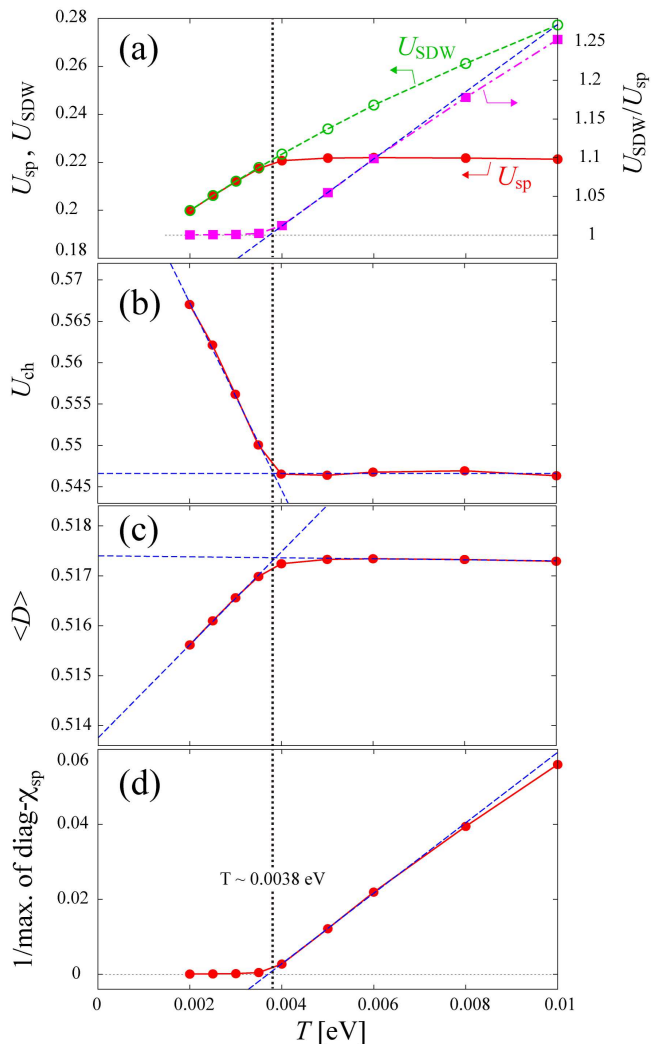


FIG. 6: (color online) Temperature dependence of (a) U_{sp} and U_{SDW} for left scale and $U_{\text{SDW}}/U_{\text{sp}}$ for right scale, (b) U_{ch} , (c) double occupancy $\langle D \rangle$, and (d) maximum value of the diagonalized spin susceptibility for the model of the I_3 salt. Blue dashed lines represents the line extrapolating the each values and black dotted lines are about $T = 0.0038\text{ eV}$.

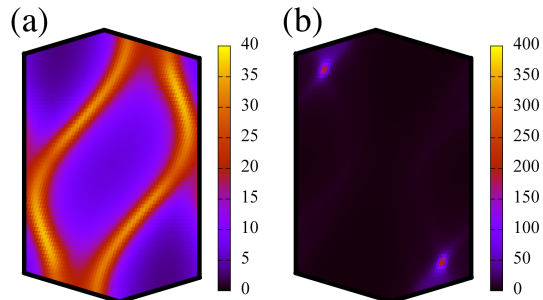


FIG. 7: (color online) (a) The absolute value of the Green's function and (b) the diagonalized spin susceptibility for the model of the I_3 salt at $T = 0.004\text{eV}$.

stronger molecular dimerization, all the quantities should

approach the values close to those of the SbF_6 salt when the dimerization is reduced hypothetically in the model of the I_3 salt.

Let us now investigate the relation between the electron correlation and the dimerization. Figure 8 (a) shows the local vertex of the spin part U_{sp} and the critical on-site interaction for the magnetic order U_{SDW} as a function of t_{p2}/t_{p1} in the model of the I_3 salt, also shows them for the SbF_6 salt at the point corresponding t_{p2}/t_{p1} , where we take $T = 0.004$ eV. Decreasing the dimerization (increasing t_{p2}/t_{p1}), U_{sp} gradually differs from U_{SDW} , which expects that increasing the t_{p2}/t_{p1} suppresses the maximum value of the spin susceptibility. In contrast to the temperature dependence, decreasing the dimerization increases U_{ch} as seen in Fig. 8 (b), although U_{sp} differs from the U_{SDW} . In Fig. 8 (c), the double occupancy $\langle D \rangle$ monotonically increases with decreasing the dimerization, which can be understood as the suppression of the magnetic localization. This tendency is confirmed by the deviation of U_{sp} from U_{SDW} . Figure 8 (d) shows the maximum value of the spin susceptibility as a function of t_{p2}/t_{p1} . Decreasing the dimerization from the actual value of the I_3 salt quickly suppresses the spin susceptibility, and that of the I_3 salt takes almost the same value as that of the SbF_6 salt around the same strength of the dimerization.

From the t_{p2}/t_{p1} dependence in Fig. 8, we can say that the electron correlation in the I_3 salt is stronger than in the SbF_6 salt due to the strong dimerization. We therefore conclude that the difference of the ground state between the two salts, namely, insulating for the I_3 salt and superconducting for the SbF_6 salt, originates from the strength of the dimerization, which affects the electron correlation. Applying the pressure to the I_3 salt reduces the dimerization, resulting in the metallicity, and hence the superconductivity appears.

IV. CONCLUSION

In the present study, we have performed first principles band calculations and have derived the effective tight-binding models of $\beta\text{-(BDA-TTP)}_2\text{I}_3$ and $\beta\text{-(BDA-TTP)}_2\text{SbF}_6$. The band structures and the Fermi surface between the I_3 and SbF_6 salts are apparently different although only the anion differs. The derived tight-binding models, which accurately reproduce the first principles band structures of the two salts, show that the differences between the two salts comes mainly from the strength of the dimerization.

As for the effect of the electron correlation, we have presented the TPSC results for quantities such as the spin susceptibility in the Hubbard model for the two salts. The TPSC results show that the electron correlation becomes stronger upon lowering the temperature and/or increasing the dimerization strength. Then, we have hypothetically reduced the strength of the dimerization in the I_3 salt to that of the SbF_6 salt, where all the calcu-

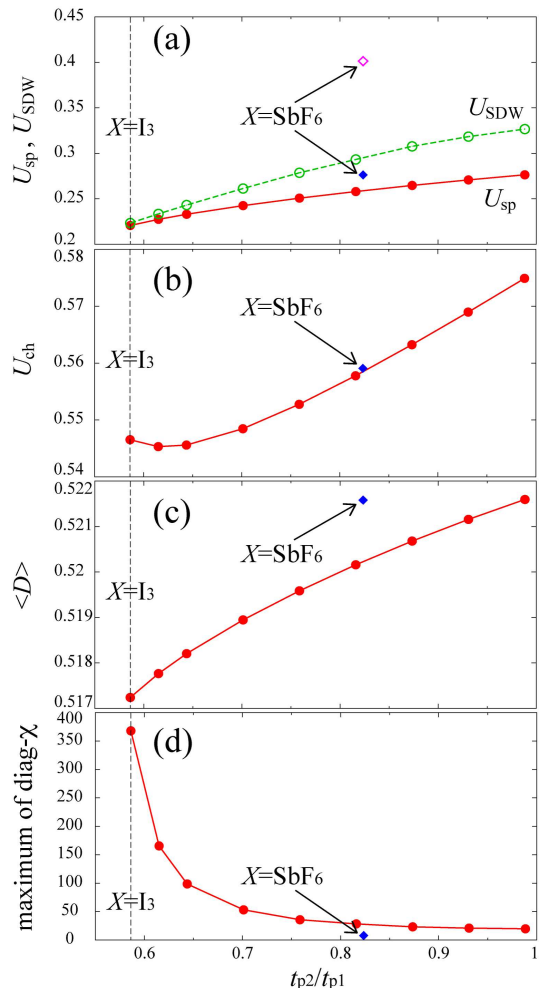


FIG. 8: (color online) The strength of the dimerization t_{p2}/t_{p1} dependence of (a) U_{sp} and U_{SDW} , (b) U_{ch} , (c) double occupancy $\langle D \rangle$, and (d) maximum value of the diagonalized spin susceptibility for the model of the I_3 salt with $U_0 = 0.8\text{eV}$ and $T = 0.004\text{eV}$. The each values on the SbF_6 salt with same U and T are also shown in the corresponding figures.

lated quantities tend to become similar to those of the SbF_6 salt. Thus, we conclude that the electron correlation in the I_3 salt is stronger than the SbF_6 salt due to the strong dimerization. The expected stronger correlation in the I_3 salt is at least qualitatively consistent with a recent experimental observation that the material is a Mott insulator, which is a hallmark of strong correlation, and exhibits a magnetic transition at low temperature³¹. Applying the pressure to the I_3 salt reduces the dimerization, which weakens the electron correlation, and hence the superconductivity appears as in the SbF_6 salt.

In the present study, we have considered only the on-site (intra-molecular) electron-electron interaction. It remains an interesting future problem to study the effect of the off-site interactions. In fact, it has been known that in organic conductors having quarter-filled bands, the Mott insulating state often competes with the charge

ordering and/or charge-density-wave states³². It is an interesting issue to investigate how such interactions would affect the insulating properties as well as the mechanism of the superconductivity.

Acknowledgment

We thank T. Isono for showing the latest experimental data. This work is supported by Grant-in-Aid for

Scientific Research from the Ministry of Education, Culture, Sports, Science and Technology of Japan, and from the Japan Society for the Promotion of Science. Part of the calculation has been performed at the facilities of the Supercomputer Center, ISSP, University of Tokyo.

-
- * Electronic address: aizawa@kanagawa-u.ac.jp
- ¹ J. S. Zambounis, C. W. Mayer, K. Hauenstein, B. Hilti, W. Hofherr, J. Pfeiffer, M. Bürkle, and G. Rihs, *Adv. Matter.* **4**, 33 (1992).
 - ² S. Kimura, T. Maejima, H. Suzuki, R. Chiba, H. Mori, T. Kawamoto, T. Mori, H. Moriyama, Y. Nishio, and K. Kajita, *Chem. Commun.*, 2454 (2004).
 - ³ J. Yamada, H. Akutsu, H. Nishikawa, and K. Kikuchi, *Chem. Rev.* **104**, 5057 (2004).
 - ⁴ J. Yamada, K. Fujimoto, H. Akutsu, S. Nakatsuji, A. Miyazaki, M. Aimatsu, S. Kudo, T. Enoki, and K. Kikuchi, *Chem. Commun.*, 1331 (2006).
 - ⁵ K. Kikuchi, T. Isono, M. Kojima, H. Yoshimoto, T. Kodama, W. Fujita, K. Yokogawa, H. Yoshino, K. Murata, T. Kaihatsu, H. Akutsu, and J. Yamada, *J. Am. Chem. Soc.* **133**, 19590 (2011).
 - ⁶ H. Ito, T. Ishihara, H. Tanaka, S. Kuroda, T. Suzuki, S. Onari, Y. Tanaka, J. Yamada, and K. Kikuchi, *Phys. Rev. B* **78**, 172506 (2008).
 - ⁷ Y. Nonoyama, Y. Maekawa, A. Kobayashi, Y. Suzumura, and J. Yamada, *J. Phys.: Conf. Ser.* **132**, 012013 (2008).
 - ⁸ J. Yamada, M. Watanabe, H. Akutsu, S. Nakatsuji, H. Nishikawa, I. Ikemoto, and K. Kikuchi, *J. Am. Chem. Soc.* **123**, 4174 (2001).
 - ⁹ E. S. Choi, E. Jobilong, A. Wade, E. Goetz, J. S. Brooks, J. Yamada, T. Mizutani, T. Kinoshita, and M. Tokumoto, *Phys. Rev. B* **67**, 174511 (2003).
 - ¹⁰ S. Yasuzuka, H. Koga, Y. Yamamura, K. Saito, S. Uji, T. Terashima, H. Aizawa, K. Kuroki, M. Tsuchiizu, H. Akutsu, and J. Yamada, *J. Phys. Soc. Jpn.* **81**, 035006 (2012).
 - ¹¹ Y. Shimojo, T. Ishiguro, T. Toita, and J. Yamada, *J. Phys. Soc. Jpn.* **71**, 717 (2002).
 - ¹² M. A. Tanatar, T. Ishiguro, T. Toita, and J. Yamada, *Phys. Rev. B* **71**, 024531 (2005).
 - ¹³ K. Nomura, R. Muraoka, N. Matsunaga, K. Ichimura, and J. Yamada, *Physica B* **404**, 562 (2009).
 - ¹⁴ S. Yasuzuka, private communications.
 - ¹⁵ H. Aizawa, K. Kuroki, S. Yasuzuka, and J. Yamada, *New J. Phys.* **14**, 113045 (2012).
 - ¹⁶ Recently, several studies report that the first-principles band structure slightly differs from those obtained by the extended Hückel method^{17–19}.
 - ¹⁷ H. Kandpal, I. Opahle, Y.-Z. Zhang, H. Jeschke, and R. Valentí, *Phys. Rev. Lett.* **103**, 067004 (2009).
 - ¹⁸ Y. Nagai, H. Nakamura, and M. Machida, *Phys. Rev. B* **83**, 104523 (2011).
 - ¹⁹ P. Alemany, J.-P. Pouget, and E. Canadell, *Phys. Rev. B* **89**, 155124 (2014).
 - ²⁰ Y. Nonoyama, Y. Maekawa, A. Kobayashi, Y. Suzumura, and H. Ito, *J. Phys. Soc. Jpn.* **77**, 094703 (2008).
 - ²¹ T. Suzuki, S. Onari, H. Ito, and Y. Tanaka, *J. Phys. Soc. Jpn.* **80**, 094704 (2011).
 - ²² P. Blaha, K. Schwarz, G. K. H. Madsen, D. Kvasnicka, J. Luitz In WIEN2K, An Augmented Plane Wave + Local Orbitals Program for Calculating Crystal Properties, (Karlheinz Schwarz/ Techn. Universität Wien, Wien, Austria, 2001).
 - ²³ Y. M. Vilck, A. -M. S. Tremblay, *J. Phys. I France* **7**, 1309 (1997).
 - ²⁴ J. Otsuki, *Phys. Rev. B* **85**, 104513 (2012).
 - ²⁵ S. Arya, P. V. Sriluckshmy, S. R. Hassan, and A. -M. S. Tremblay, arXiv:1504.06373.
 - ²⁶ H. Miyahara, R. Arita, and H. Ikeda, *Phys. Rev. B* **87**, 045113 (2013).
 - ²⁷ For correspondence with our previous study¹⁵, the lattice coordinates c and a taken in the SbF_6 salts correspond with $-c$ and $c + a$ in the I_3 salts according to the structure data for both materials.^{4,8} Similarly, the notation of the transfer energies is different. We employ the lattice coordinates and notation of the I_3 salts in this article.
 - ²⁸ H. Kino, and H. Fukuyama, *J. Phys. Soc. Jpn.* **65**, 2158 (1996).
 - ²⁹ K. Nakamura, Y. Yoshimoto, T. Kosugi, R. Arita, and M. Imada, *J. Phys. Soc. Jpn.* **78**, 083710 (2009).
 - ³⁰ K. Nakamura, Y. Yoshimoto, and M. Imada, *Phys. Rev. B* **86**, 205117 (2012).
 - ³¹ T. Isono, private communication.
 - ³² For a review, H. Seo, J. Merino, H. Yoshioka, and M. Ogata, *J. Phys. Soc. Jpn.* **75**, 051009 (2006).